Hindawi
Mathematical Problems in Engineering
Volume 2020, Article ID 2326868, 14 pages
https://doi.org/10.1155/2020/2326868

Research Article

Analysis of Rolling Force for Extra-Thick Plate with CA Criterion

Shun Hu Zhang, Lei Deng, and Peng Li

Shagang School of Iron and Steel, Soochow University, Suzhou 215021, China

Correspondence should be addressed to Shun Hu Zhang; shzhang@suda.edu.cn

Received 16 August 2020; Revised 31 October 2020; Accepted 9 November 2020; Published 21 November 2020

Academic Editor: Francisco J. Montáns

In order to solve the nonlinear integral difficulty of the Mises yield criterion, a linear yield criterion, called the collaborative approximation (CA) yield criterion, is proposed by the collaborative control method. According to the approximation method, the mathematical expression of the CA yield criterion is derived as a linear function of the three principal stresses. The theoretical results based on the yield criterion in the form of the Lode parameter are verified with the classical test data, and a good agreement is found. Meanwhile, for the purpose of proving the effectiveness of the yield criterion, its specific plastic power is derived and applied to establish the rolling force model of an extra-thick plate. In the modeling, the internal power of plastic deformation is obtained by using the derived specific plastic power, while the shear power dissipation and the frictional power dissipation are obtained by using the methods of strain vector inner product and average velocity integration. Then, the analytical solution of the rolling force is obtained and then extended to the one accounting for the temperature rise. The maximum errors of the predicted rolling torque and rolling force without considering the temperature rise are 12.72% and 11.78%, respectively, while those considering the temperature rise decrease to 3.54% and 5.23%, respectively. Moreover, the influence of relative reduction, friction factor, surface temperature, and the temperature rise of the workpiece on the theoretical results is discussed.

1. Introduction

Plastic metal forming is an effective method to produce various engineering components. To complete one metal forming process, it is better to establish a mathematical model as an adjustment basis of processing parameters. For the modeling, it is needed to establish and solve many mechanical equations. Of which, the yield criterion is one important equation that needs to be developed and applied. It can clarify the principle of material deformation, or provide the basis of establishing the critical conditions of material yield and failure, as well as to provide theoretical basis of material processing. Due to its wide range of applications, it has attracted the attention of many researchers in the fields of mechanics, mathematics, physics, materials science, and other engineering fields in recent years.

The earliest researcher on material yield is Coulomb [1]. In 1776, he put forward the maximum strength theory, which assumed that if the maximum shear stress of a material exceeds the sum of the frictional forces generated by the pressure in a plane of force, then the material will yield. Subsequently, he proposed two yield criteria which could be widely applied to isotropic materials. In 1864, Tresca [2] proposed a yield criterion in terms of basic experimental data. In his opinion, plastic deformation will occur when the maximum shear stress reaches the limit value. Later, the Tresca yield criterion was widely used. However, since the Tresca criterion did not consider the influence of the intermediate principal stress on material yield, there are still some problems in practical application. In order to further study the yield behavior of materials, Mises [3, 4] gave the same weight to the intermediate principal stress when studying the factors affecting the yield of materials. He believed that the yield of the material is the coaction of principal stresses, and the material will yield when the equivalent stress reaches a certain value. Since the Mises yield criterion is expressed in a single formula, it is easier to be used. Later, the Tresca yield criterion and the Mises yield criterion were verified by Hill [5], and he pointed out that for the stable isotropic metal materials, the Tresca yield criterion

is the lower bound yield criterion, while the Mises yield criterion is the upper bound yield criterion. However, it is difficult to be used in analyzing complex problems since its expression is nonlinear. In order to disclose the differences among various yield criteria, Haigh and Westgard [6] introduced the concept of limit surface in the three-dimensional principal stress space and provided a possibility for the visualization of the two yield criteria.

In recent years, researchers have conducted more and more studies on the yield of materials and proposed various new yield criteria for materials with different properties. To replace the Mises yield criterion for solving many complex problems, Yu [7] proposed the twin shear stress (TSS) yield criterion. Because the TSS yield criterion is a linear yield criterion, it provides a new method to analyze complex stress condition. Zhao [8, 9] verified the TSS yield criterion and pointed out that the TSS yield criterion has greater practical value in engineering application. Compared with the Mises yield criterion, Yu [10, 11] postulated that the plastic flow of the material is controlled by two large shear stresses. Based on this assumption, Yu also proposed a unified yield criterion (UYC) consisting of piecewise mathematical expressions. Li [12] proposed a generalized double τ yield criterion for metal materials. This yield criterion assumes that when the sum of the squares of the three main shear stresses at a point of the metal material reaches a certain value, then the metal material yields. Zhao [13] found the linear characteristic of the Tresca yield criterion and TSS yield criterion and proposed a mean yield (MY) criterion to replace the Mises yield criterion. Oana Cazacu [14] proposed a new yield criterion after studying the asymmetry of non-pressure-sensitive metal materials in the yield process. This yield criterion only involves one parameter and can express the yield conditions of non-pressure-sensitive metal materials after being compressed or stretched. Zhu [15] proposed an average shear stress (ASSY) yield criterion based on the Tresca and Mises yield criterion in order to predict the rupture pressure of pipes accurately during the plastic failure. Another unified yield criterion is proposed by Song [16], which can better describe the yield conditions of different types of metallic glass. In the same year, Hu [17] proposed a unified yield criterion of three shear stresses after considering the influence of shear stress acting on dodecahedral elements, which can reduce to the classic Tresca yield criterion, Mises yield criterion, and Mohr–Coulomb failure criterion. Based on many experimental results, Khan [18] proposed a yield criterion to describe the yield behavior and the asymmetric properties of tension-compression of electron beam single melt alloy Ti_6Al_4V. This yield criterion introduces a new method to explain the anisotropy and the tension and compression asymmetry so that the anisotropy parameters and the tension and compression asymmetry parameters can be determined, respectively. Banabic et al. [19] verified the prediction effect of the maximum force criterion and Marciniak–Kuczynski model on the limit forming curve of aa6016-t4 aluminum alloy and proposed the profit function of the improved model which is based on the criterion and the model. Lou [20] proposed a new uncoupled shear ductile fracture yield criterion. They also verified it by the shear test, uniaxial tensile test, plane strain tensile test, and Nakajima test. The results show that this criterion can be used to predict the ductile fracture of bulk metal forming process. Based on the experimental observation, Werber et al. [21] proposed a failure prediction criterion for the sheet forming process and described the failure surface accordingly. However, in the actual forming process, the actual effect of this failure prediction criterion needs to be evaluated.

Also, various yield criteria have been widely used in engineering applications. Kabayashi [22] and Kato [23] developed kinematically admissible velocity field for rolling modeling. Nevertheless, their model can only obtain the corresponding numerical results of rolling force and torque. Parghazeh and Haghighat [24] found that the analytical solution of drawing force is hard to be obtained due to the nonlinear expression of the Mises yield criterion. It can be seen that the development of a linear yield criterion and its specific plastic power is of great significance for obtaining analytical parameters. Recently, the rolling process has been analyzed in terms of various linear yield criteria. To improve width control of vertical rolling, Cao et al. [25] established a rolling model by using the angular bisector yield criterion. It is found that the prediction accuracy of the model is higher than that of the exist online control model. Zhang et al. [26] established a rolling model by using the equal area yield criterion and verified the model with measured data. The results show that the model has good prediction accuracy and can be used to predict the rolling force and rolling torque of hot strip rolling. By using the mean yield criterion, Liu et al. [27] established a rolling model with high accuracy, and the influence of other factors such as friction factor, reduction, and shape factor on the prediction of rolling force and rolling torque also be discussed. Using the equal area yield criterion, Wen et al. [28] established a rolling model based on a parabolic velocity field. Their results show that the predictions are closer to the actual value. In order to study the effect of uneven deformation on predicting rolling force in the heavy plate, Wang et al. [29] established a rolling model for vertical Dog-Bone rolling by using the geometrical midline (GM) yield criterion and antisymmetric velocity field. The validation result shows that this model not only has high accuracy in predicting rolling force and rolling torque but also provides a new way for width control of vertical rolling. In the author's previous research [30, 31], the geometric approach (GA) yield criterion was proposed and proved to be effective in the prediction model of rolling force. However, there are still some gaps between their predictions and actual data by using the mentioned yield criteria since they are not the best one that approximates the Mises yield criterion. It should also be noted that there also exist reports on the mechanics of micro-nano sized plates. Akgöz and Civalek [32] analyzed the functionally graded microbeams (FGMs) based on the strain gradient theory. The related boundary conditions and buckling response of FGMs are investigated. Subsequently, they [33] also developed a microstructure-dependent sinusoidal plate model based on modified strain gradient theory and sinusoidal shear deformation theory. The model not only can consider

the effects of shear deformation but also can capture the size effects. Ebrahimi et al. [34] established a nonlocal couple stress theory to describe the static stability and free vibration characteristics of FG nanobeams. In the theory, they introduced two parameters to capture the size effects much accurately. The parametric study includes several parameters on natural frequencies and buckling loads of FG nanobeams in details, which can provide experience for researchers in the field.

In this paper, for solving the nonlinear integral difficulty of the Mises yield criterion, the locus of the Mises yield criterion on the π plane is linearly treated, and a linear yield criterion is proposed. Moreover, the corresponding specific plastic power is derived. For proving the effectiveness, the yield criterion is verified with the experimental data. Its specific plastic power is used to analyze the rolling force and rolling torque as an application example. Moreover, the effect of temperature rise on the rolling force is discussed.

2. Collaborative Approximation Yield Criterion

2.1. Yield Equation and Its Geometrical Description. The classical Tresca, Mises, and TSS (twin shear stress) yield criteria can be graphically displayed on the π plane, as shown in Figure 1. It can be seen that the yield locus of the Mises yield criterion is a circle, and the yield loci of the Tresca and TSS yield criteria are the inscribed and circumscribed hexagons.

As demonstrated before, the mechanical calculation based on the Tresca yield criterion always provides conservative results, whereas the TSS yield criterion often provides excessive results. Thus, it is suggested to construct a straight line between them and can approach well with the Mises locus since the Mises yield criterion has been proved to be used well in most cases. In order to clarify the construction method of a new yield criterion, a twelfth of the yield loci in Figure 1 are selected for analysis, as shown in Figure 2.

In the error triangle $\Delta B'FB$, there can exist a removable point E along the FB. The straight line $B'E$ as the new yield locus varies as the point E moves. When the intersection point G occurs, a high approximation with respect to the Mises arc can be obtained. In such case, there are the maximum errors in the upper and lower parts, denoted by the length error IM and DE. As the point E moves from D to B, the length error DE increases, while the length error IM decreases. It can be seen that the overall approximation should depend on these two errors. Therefore, it is necessary to collaboratively control them. It is found that when the IM is equal to DE, the overall error between the new locus $B'E$ and the Mises arc reaches the minimum, and the approximation is the best. This approximate method is defined as the collaborative control method. Based on this idea, a new yield criterion can be developed by finding the position of the point E by letting $DE = IM$, and this yield criterion can be called the collaborative approximation yield criterion, abbreviated as the CA yield criterion.

The coordinate system is established at the point O as the origin, and the coordinates of the points I, G, and B' are set

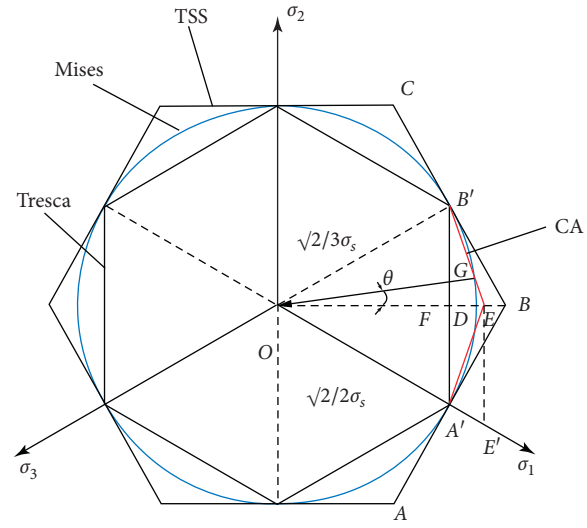

Figure 1: Linear approximation of the Mises locus on π plane.

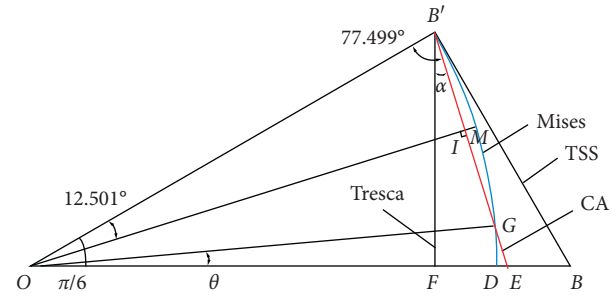

Figure 2: The locus of the CA yield criterion in the error triangle $\Delta B'FB$.

to (x_I, y_I), (x_G, y_G), and $(x_{B'}, y_{B'})$, respectively. Take notice of $OB' = OD = (\sqrt{6}\,\sigma_s/3)$ (σ_s is the yield strength), $OF = (\sigma_s/\sqrt{2})$, and $B'F = (\sigma_s/\sqrt{6})$ and assume the unknown length $OE = c$, then the equation of the $B'E$ can be expressed by $y = ax + b$ (where the symbols a, b, and c denote the undetermined coefficients). Substituting the point B' $((\sigma_s/\sqrt{2}), (\sqrt{6}/\sigma_s))$ and the point E $(c, 0)$ into this equation, it results in

$$y = \frac{\sigma_s}{\sqrt{3}\left(\sigma_s - \sqrt{2}\,c\right)}(x - c). \tag{1}$$

On the other hand, the equation of the Mises arc can be expressed by

$$x^2 + y^2 = \left(\frac{\sqrt{6}}{3}\sigma_s\right)^2. \tag{2}$$

By combining equations (1) and (2), the abscissa x_G of the intersection point G can be solved, which is

$$x_G = \frac{\sqrt{q^2\left(6 - 9c^2\right) + 6\sigma_s} + 3q^2c}{3\left(q^2 + 1\right)}, \tag{3}$$

where $q = (\sigma_s/\sqrt{3}\,(\sigma_s - \sqrt{2}\,c))$.

According to the geometrical relation in Figure 2, it can be seen that the abscissa x_I of the point I can be solved by

$$x_I = \frac{x_G + x_{B'}}{2} = \frac{2\sqrt{q^2\left(6 - 9c^2\right) + 6\sigma_s} + 3q^2 c}{3\left(q^2 + 1\right)} + \sqrt{2}. \quad (4)$$

Substitute equation (4) into (1), and then the vertical coordinate y_I can be obtained:

$$y_I = q\left[\frac{2\sqrt{q^2\left(6 - 9c^2\right) + 6\sigma_s} + 3q^2 c}{3\left(q^2 + 1\right)} + \sqrt{2} - c\right]. \quad (5)$$

Thus, the length errors IM and DE can be calculated as follows:

$$\begin{aligned} \mathrm{IM} &= \mathrm{OM} - \mathrm{OI} = \frac{\sqrt{6}}{3}\sigma_s - \sqrt{x_I^2 + y_I^2}, \\ \mathrm{DE} &= \mathrm{OE} - \mathrm{OD} = c - \frac{\sqrt{6}}{3}\sigma_s. \end{aligned} \quad (6)$$

By letting IM = DE, it results in

$$c - \frac{2\sqrt{6}}{3}\sigma_s + \sqrt{x_I^2 + y_I^2} = 0. \quad (7)$$

By solving equation (7) with the successive approximation method from the abscissa of the point D to that of the point B, it leads to

$$c = 0.8358\sigma_s. \quad (8)$$

Thus, the side lengths EF, $B'E$, DE, and OI and the angles $\angle\alpha$, $\angle OB'E$, $\angle OEB'$, and $\angle B'OI$ can be calculated as follows:

$$\left.\begin{aligned} EF &= OE - OF = 0.8358\sigma_s - \frac{1}{\sqrt{2}}\sigma_s = 0.1287\sigma_s \\ B'E &= \sqrt{B'F^2 + FE^2} = 0.4280\sigma_s \\ DE &= OE - OD = 0.0193\sigma_s \\ OI &= OB' \cdot \cos\angle B'OI = 0.7971\sigma_s \end{aligned}\right\},$$
$$\left.\begin{aligned} \angle\alpha &= \arctan\left(\frac{EF}{B'F}\right) = 17.499^\circ \\ \angle OB'E &= 60^\circ + \angle\alpha = 77.499^\circ \\ \angle OEB' &= 180^\circ - 30^\circ - 77.499^\circ = 72.501^\circ \\ \angle B'OI &= 90^\circ - \angle OB'E = 12.501^\circ \end{aligned}\right\}. \quad (9)$$

The relative perimeter error Δ_C and the relative area error Δ_A between the CA yield locus and the Mises circle can be deduced

$$\Delta_C = \frac{\left(C_{\mathrm{CA}} - C_{\mathrm{Mises}}\right)}{C_{\mathrm{Mises}}} = 0.124\%, \quad (10)$$

$$\Delta_A = \frac{\left(S_{\mathrm{CA}} - S_{\mathrm{Mises}}\right)}{S_{\mathrm{Mises}}} = -2.235\%, \quad (11)$$

where C_{CA} and C_{Mises} are the perimeters and S_{CA} and S_{Mises} are the areas.

It can be seen from equations (10) and (11) that the approximation is very well since both the two geometrical errors are very small. Therefore, the criterion can be used in the calculation of mechanical parameters during plastic forming. In other words, the effect of the two length errors on the further errors during the subsequent analysis of plate rolling is very small and can be ignored.

Hereby, the locus of the CA yield criterion is a dodecagon with equilateral side and nonequilateral angle. It intersects with the Mises locus and generates twelve intersection points. The six vertices of the locus are on the Mises circle, and the vertex angle are 154.998°. The other six vertices are located on the outer side of the Mises circle, and the vertex angles are 145.002°. Each length of the dodecagon is $0.4280\sigma_s$.

The following section is the derivation of the CA yield equation. The projection of the principal stress component σ_1 on the π plane is shown in Figure 3.

The stress components of the point E can be obtained from Figures 1 and 3:

$$\left.\begin{aligned} \sigma_1 &= \sqrt{\frac{3}{2}}OE' = \frac{\sqrt{6}}{2} \times \frac{OE}{\cos 30^\circ} = \sqrt{2}\,OE = 1.182\sigma_s \\ \sigma_3 &= 0 \\ \sigma_2 &= \frac{\sigma_1 + \sigma_3}{2} = 0.591\sigma_s \end{aligned}\right\}. \quad (12)$$

It can be supposed that the line $A'E$ satisfies the following equation:

$$\sigma_1 - a_1\sigma_2 - a_2\sigma_3 - d = 0. \quad (13)$$

It is noted that $d = \sigma_s$ and $a_1 + a_2 = 1$ when the material yields. Substituting the stress components into equation (13), one can obtain

$$\begin{aligned} a_1 &= 0.308, \\ a_2 &= 0.692. \end{aligned} \quad (14)$$

Thus, equation (13) can be determined as

$$\sigma_1 - 0.308\sigma_2 - 0.692\sigma_3 = \sigma_s, \quad \text{if } \sigma_2 \le \frac{1}{2}(\sigma_1 + \sigma_3). \quad (15)$$

Similarly, the equation of the locus $B'E$ can be determined as

$$0.692\sigma_1 + 0.308\sigma_2 - \sigma_3 = \sigma_s, \quad \text{if } \sigma_2 \ge \frac{1}{2}(\sigma_1 + \sigma_3), \quad (16)$$

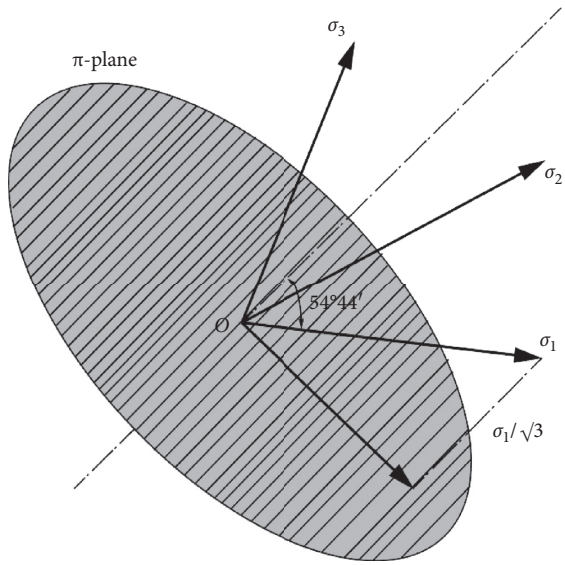

Figure 3: The projection of σ_1 onto the π plane.

where equations (15) and (16) are the mathematical expressions of the CA yield criterion. It is shown that if the stress components σ_1, σ_2, and σ_3 obey the linear combination according to coefficient 1, 0.308, and 0.692 or 0.692, 0.308, and 1, then the material yields.

From equation (12), it can be derived that $\tau_s = ((\sigma_1 - \sigma_3)/2) = 0.591\sigma_s$. This indicates that when the shear yield stress of the material reaches $0.591\sigma_s$, the material will yield. The yield stress σ_s can be determined by uniaxial tensile or compressive tests. The comparison with the above yield criterion shows that the yield shear stress of the CA yield criterion is close to the Mises shear yield stress $\tau_s = 0.577\sigma_s$ and lies in between the Tresca shear yield stress $\tau_s = 0.5\sigma_s$ and the TSS shear yield stress $\tau_s = 0.667\sigma_s$.

2.2. Specific Plastic Power. It is known that the stress σ_{ij} should satisfy $f(\sigma_{ij}) = 0$ and the strain rate $\dot{\varepsilon}_{ij}$ should satisfy the flow law $\dot{\varepsilon}_{ij} = d\lambda(\partial f/\partial\sigma_{ij})$ [35]. If we assume $\lambda \geq 0$ and $\mu \geq 0$, then it can be obtained from equations (15) and (16) that

$$\begin{aligned}&\dot{\varepsilon}_1 : \dot{\varepsilon}_2 : \dot{\varepsilon}_3 = 1 : (-0.308) : (-0.692) = \lambda : (-0.308)\lambda : (-0.692)\lambda,\\ &\dot{\varepsilon}_1 : \dot{\varepsilon}_2 : \dot{\varepsilon}_3 = 0.692 : 0.308 : (-1) = 0.692\mu : 0.308\mu : (-\mu).\end{aligned} \tag{17}$$

The linear combination of the above two results leads to

$$\dot{\varepsilon}_1 : \dot{\varepsilon}_2 : \dot{\varepsilon}_3 = (\lambda + 0.692\mu) : 0.308(\mu - \lambda) : [-(0.692\lambda + \mu)]. \tag{18}$$

Take $\dot{\varepsilon}_1 = \lambda + 0.692\mu$, it leads to

$$\begin{aligned}\dot{\varepsilon}_2 &= 0.308(\mu - \lambda),\\ \dot{\varepsilon}_3 &= -(0.692\lambda + \mu).\end{aligned} \tag{19}$$

Since $\dot{\varepsilon}_{\max} = \dot{\varepsilon}_1$ and $\dot{\varepsilon}_{\min} = \dot{\varepsilon}_3$, it can be obtained that

$$\begin{aligned}\dot{\varepsilon}_{\max} - \dot{\varepsilon}_{\min} &= 1.692(\lambda + \mu),\\ (\lambda + \mu) &= \frac{1000}{1692}(\dot{\varepsilon}_{\max} - \dot{\varepsilon}_{\min}).\end{aligned} \tag{20}$$

At the vertex E, note that $\sigma_2 = ((\sigma_1 + \sigma_3)/2)$; it can be obtained from equations (15) and (16) that

$$\begin{aligned}1.692\sigma_1 - 1.692\sigma_3 &= 2\sigma_s,\\ \sigma_1 - \sigma_3 &= \frac{2000}{1692}\sigma_s.\end{aligned} \tag{21}$$

Therefore, the specific plastic power can be obtained from equations (20) and (21).

$$\begin{aligned}D(\dot{\varepsilon}_{ij})_{\mathrm{CA}} &= \sigma_1\dot{\varepsilon}_1 + \sigma_2\dot{\varepsilon}_2 + \sigma_3\dot{\varepsilon}_3 = \sigma_1\dot{\varepsilon}_1 + \frac{\sigma_1 + \sigma_3}{2}\dot{\varepsilon}_2 + \sigma_3\dot{\varepsilon}_3,\\ &= 0.846(\sigma_1 - \sigma_3)(\mu + \lambda),\\ &= \frac{1692}{2000} \times \frac{2000}{1692}\sigma_s \times \frac{1000}{1692}(\dot{\varepsilon}_{\max} - \dot{\varepsilon}_{\min}),\\ &= \frac{1000}{1692}\sigma_s(\dot{\varepsilon}_{\max} - \dot{\varepsilon}_{\min}),\\ &= 0.591\sigma_s(\dot{\varepsilon}_{\max} - \dot{\varepsilon}_{\min}).\end{aligned} \tag{22}$$

As can be seen from equation (22), the derived specific plastic power is a linear function of σ_s, $\dot{\varepsilon}_{\max}$, and $\dot{\varepsilon}_{\min}$, which is beneficial to obtain analytical solutions of complex mechanical problems.

3. Validation and an Application Example

3.1. Experimental Validation. The Tresca yield criterion, Mises yield criterion, TSS yield criterion, and the present CA yield criterion rewritten with Lode parameter $\mu_d = (2\sigma_2 - \sigma_3 - \sigma_1/\sigma_1 - \sigma_3)$[36] can be obtained as follows:

$$\begin{aligned}\text{Tresca: } &\frac{\sigma_1 - \sigma_3}{\sigma_s} = 1,\\ \text{Mises: } &\frac{\sigma_1 - \sigma_3}{\sigma_s} = \frac{2}{\sqrt{3 + u_d^2}},\\ \text{TSS: } &\frac{\sigma_1 - \sigma_3}{\sigma_s} = \begin{cases}\dfrac{4 + \mu_d}{3}, & -1 \leq \mu_d \leq 0,\\ \dfrac{4 - \mu_d}{3}, & 0 \leq \mu_d \leq 1,\end{cases}\\ \text{CA: } &\frac{\sigma_1 - \sigma_3}{\sigma_s} = \begin{cases}\dfrac{2000 + 308\mu_d}{1692}, & -1 \leq \mu_d \leq 0,\\ \dfrac{2000 - 308\mu_d}{1692}, & 0 \leq \mu_d \leq 1.\end{cases}\end{aligned} \tag{23}$$

Figure 4 compares the Tresca yield criterion, Mises yield criterion, TSS yield criterion, and the CA yield criterion with

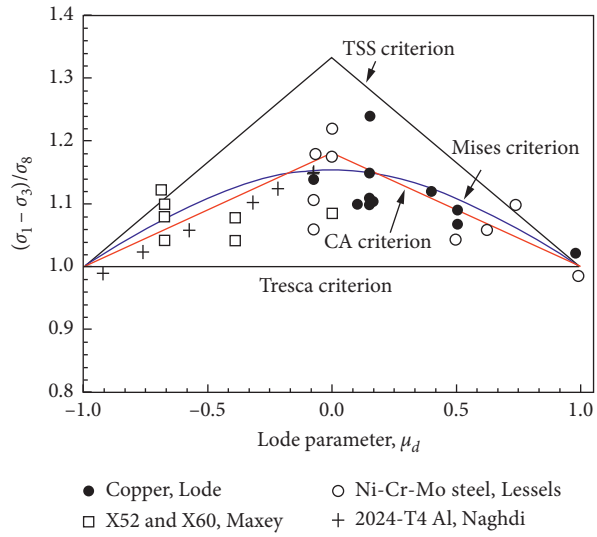

Figure 4: Comparison of yield criteria with available experimental data in reference to Lode stress parameter.

the experimental data of copper [36], Ni – Cr – Mo steel [37], 2024 – T4 aluminum [38], and X52, X60 pipeline steel [39].

As can be seen from Figure 4, the TSS yield criterion gives the upper limit of experimental data, while the Tresca yield criterion gives the lower limit. The results given by the CA yield criterion are between the above two, which are in good agreement with experimental data and have a high approximation to the Mises yield criterion.

In the plane stress state ($\sigma_3 = 0$), the classical biaxial stress experimental data of (σ_2/σ_s) versus (σ_1/σ_s) are used to compare the present CA yield locus with the loci of the Tresca yield criterion, Mises yield criterion, and TSS yield criterion, as shown in Figures 5(a) and 5(b). In Figure 5(a), the experimental data are obtained by Lode [36] under various axial loads for thin-walled steel pipe, copper pipe, and nickel pipe. The data in Figure 5(b) are obtained through the biaxial stress test under the combined action of the tension and internal pressure of steel tubes, in which the used materials are Mi-Cr-Mo steel [37], AISI 1023 steel [40], low-carbon steel [41], structural steel [42], and pipeline steel [39].

It can be seen that the Tresca and TSS yield loci are the upper and lower bounds, respectively, and the proposed CA yield criterion locus lies in between them and closes to the Mises yield locus, which indicates that the present yield criterion approximates well with the Mises yield criterion.

3.2. Rolling Force Model of Ultra-Heavy Plate Based on the CA Yield Criterion. The following is an example of modeling the rolling force of an extra-thick plate to show the superiority of the proposed yield criterion. Considering the symmetry of the rolling workpiece, only (1/4) is taken in the analysis.

3.2.1. Rolling Velocity Field. In this paper, it is assumed that the deformation of the workpiece is uniform and the entrance and exit sections remain planes. Due to the high temperature of the hot rolling process, the roller is assumed to be rigid and the effect of elastic flattening on rolling torque and rolling force is not considered. After the first shaping rolling pass, it turns into the broadside rolling stage. Although the shape factor $(l/2h) \le 1$, the workpiece width-thickness ratio (b/h) is much larger than 10, and the width change of the workpiece in the longitudinal direction can be ignored, so the deformation in the subsequent rolling stage belongs to the plane deformation. The schematic diagram of the rolled part is shown in Figure 6, in which the initial plate thickness $2h_0$ is rolled into the finished product with the thickness of $2h_1$. The origin of coordinates is located at the symmetric center of the entrance plane. According to the geometric relationship in Figure 6, the contact arc equation, parametric equation, and the first and second derivatives are as follows:

$$\begin{aligned} z = h_x &= R + h_1 - \left[R^2 - (l-x)^2\right]^{1/2} \text{or } z = h_\alpha \\ &= R + h_1 - R\cos\alpha, \\ l - x &= R\sin\alpha, \\ \mathrm{d}x &= -R\cos\alpha \mathrm{d}\alpha, \\ h_x' &= -\tan\alpha, \\ h_x'' &= \left(R\cos^3\alpha\right)^{-1}, \end{aligned} \tag{24}$$

where R is the radius of the roller; α is the contact angle of the deformation zone; and θ is the bite angle.

The geometric boundary condition shown in Figure 6 is

$$\begin{cases} x = 0\,(\alpha = \theta), \\ h_x = h_\alpha = h_\theta = h_0, \\ h_x' = -\tan\alpha \\ x = l\,(\alpha = 0), \\ h_x = h_\alpha = h_1, \\ h_x' = 0. \end{cases} \tag{25}$$

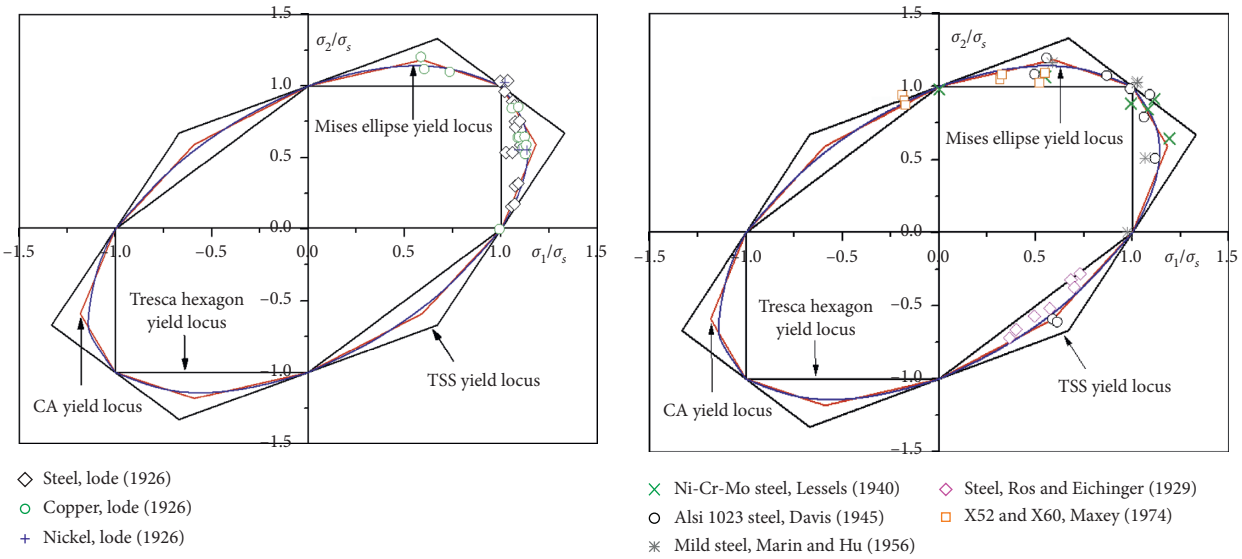

FIGURE 5: Comparison of the classical biaxial stress experimental data of initial stresses with Mises locus, Tresca locus, TSS locus, and CA locus.

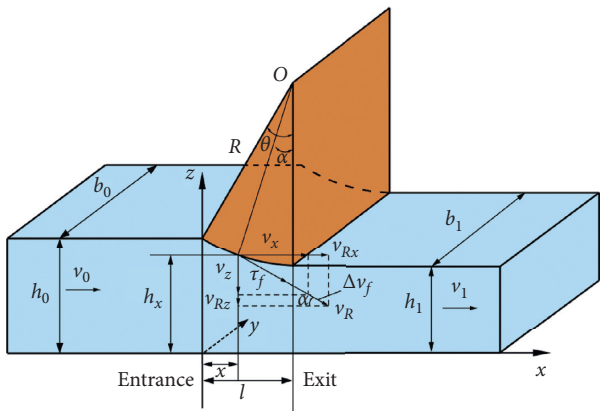

FIGURE 6: The rolling deformation zone.

For the shape factor $(l/(2h)) \le 1$ and the width-to-thickness rate $(b/h) \gg 10$, the width function b_x from the entrance to the exit can be regarded as a constant and can be obtained as

$$y = b_x = \frac{b_0 + b_1}{2} = b. \tag{26}$$

Due to the simplification of the plate width, the rolling process can be viewed as a two dimensional problem, and the rolling velocity field proposed by Kobayashi in 1975 [43] can be simplified by replacing b_x by b. Then, the velocity field for the present rolling process can be expressed as

$$\begin{aligned} v_x &= \frac{U}{h_x b}, \\ v_z &= v_x \frac{h_x'}{h_x} z, \\ v_y &= 0. \end{aligned} \tag{27}$$

According to the Cauthy formula [44], the corresponding strain rate components can be obtained as follows:

$$\begin{aligned} \dot{\varepsilon}_x &= -v_x \frac{h_x'}{h_x}, \\ \dot{\varepsilon}_z &= v_x \frac{h_x'}{h_x}, \\ \dot{\varepsilon}_y &= 0, \\ \dot{\varepsilon}_{xz} &= \frac{z}{2} v_x \left[\frac{h_x''}{h_x} - 2\left(\frac{h_x'}{h_x} \right)^2 \right], \\ \dot{\varepsilon}_{xy} &= \dot{\varepsilon}_{yz} = 0, \end{aligned} \tag{28}$$

where U is the volume flow rate in the deformation zone:

$$U = v_0 h_0 b = v_x h_x b = v_R \cos\alpha_n b \left(R + h_1 - R\cos\alpha_n \right) = v_1 h_1 b. \tag{29}$$

In equations (27) and (28), there are $\dot{\varepsilon}_x + \dot{\varepsilon}_y + \dot{\varepsilon}_z = 0$; $x = 0$, $v_x = v_0$; $x = l$, $v_x = v_1$; $z = 0, v_z = 0$; and $z = h_x$, $v_z = -v_x \tan\alpha$. Therefore, the simplified velocity field still satisfies the kinetically admissible condition.

3.2.2. The Internal Power of Plastic Deformation. For solving the difficultly of integrating the internal power of plastic deformation due to the Mises yield criterion, the proposed CA yield criterion is introduced by using the replacement method of the specific plastic power, that is to replace $D(\dot{\varepsilon}_{ij})_{\text{Mises}}$ by $D(\dot{\varepsilon}_{ij})_{\text{CA}}$ shown in equation (22). Noting that there are $\dot{\varepsilon}_{\max} = \dot{\varepsilon}_x = \dot{\varepsilon}_1$ and $\dot{\varepsilon}_{\min} = \dot{\varepsilon}_z = \dot{\varepsilon}_3$in equation (28), then substituting them into equation (22), and integrating in the deformation zone, one can obtain

$$\begin{aligned} N_d &= \int_v D\left(\dot{\varepsilon}_{ij}\right)_{\mathrm{CA}} \mathrm{d}V = 4\int_0^l\int_0^b\int_0^{h_x} 0.591\sigma_s \\ &\quad \cdot \left(\dot{\varepsilon}_{\max} - \dot{\varepsilon}_{\min}\right)\mathrm{d}x\mathrm{d}y\mathrm{d}z, \\ &= 2.364\sigma_s \int_0^l\int_0^b\int_0^{h_x}\left(-2\nu_x\frac{h_x'}{h_x}\right)\mathrm{d}x\mathrm{d}y\mathrm{d}z, \\ &= -4.728\sigma_s U\int_0^l \frac{h_x'}{h_x}\mathrm{d}x, \\ &= 4.728\sigma_s U\ln\frac{h_0}{h_1}. \end{aligned} \tag{30}$$

Due to the replacement, the explicit expression of the internal power of plastic deformation can be obtained, which has overcome the solution difficulty due to the nonlinear Mises specific plastic power.

3.2.3. The Frictional Power Dissipation. The frictional power dissipation consumed on the contact surface between the rollers and the workpiece is

$$N_f = 4\int_F \tau_f \Delta v_f \mathrm{d}F, \tag{31}$$

where $\tau_f = mk$ is the friction shear stress, $k = (\sigma_s/\sqrt{3})$ is shear yield strength, Δv_f is the velocity discontinuity, and $\mathrm{d}F$ is the infinitesimal area, which can be expressed as

$$\begin{cases} \Delta v_f = v_R - v_x\sqrt{1+h_x'^2} = v_R - v_x\sec\alpha, \\ \mathrm{d}F = \sqrt{1+h_x'^2}\,\mathrm{d}x\mathrm{d}y = \sec\alpha\mathrm{d}x\mathrm{d}y, \end{cases} \tag{32}$$

As can be seen from Figure 6, the direction cosines formed by Δv_f and the coordinate axes are, respectively,

$$\begin{aligned} \cos\alpha &= \pm\frac{\sqrt{R^2-(l-x)^2}}{R}, \\ \cos\beta &= 0, \\ \cos\gamma &= \pm\frac{(l-x)}{R} = \sin\alpha. \end{aligned} \tag{33}$$

By using the collinear vector inner product method [45], the integration of equation (31) can be converted to

$$\begin{aligned} N_f &= 4\int_0^l\int_0^b \tau_f\Delta v_f\sqrt{1+h_x'^2}\mathrm{d}x\mathrm{d}y, \\ &= 4b\int_0^l\left(\tau_{f_x}\Delta v_x + \tau_{f_z}\Delta v_z\right)\sec\alpha\mathrm{d}x, \\ &= 4mkb\int_0^l\left(\Delta v_x\cos\alpha + \Delta v_z\cos\gamma\right)\sec\alpha\mathrm{d}x, \end{aligned} \tag{34}$$

where Δv_x and Δv_z are the velocity discontinuity along the x axis and z axis.

Substituting equation (33) into (34), one can obtain

$$N_f = \frac{4m\sigma_s}{\sqrt{3}}\left[bv_R R\left(\theta - 2\alpha_n\right) + \frac{UR}{h_m}\ln\frac{\tan^2\left((\pi/4)+(\alpha_n/2)\right)}{\tan\left((\pi/4)+(\theta/2)\right)}\right], \tag{35}$$

where $h_m = \overline{h}_x = (h_0 + h_1/2)$ is the mean thickness of the plate.

3.2.4. The Shear Power Dissipation Dissipation. According to equation (27), $x = l$, $h_x' = b_x' = 0$, and $v_y|_{x=l} = v_z|_{x=l} = 0$. Therefore, no shear power is consumed at the exit section of the deformation zone. The shear power dissipation consumed at the entrance section N_{s_0} is the total shear power N_s. The velocity discontinuity and the shear power dissipation can be obtained as

$$\left|\Delta v_s\right|_{x=0} = \sqrt{\Delta v_z^2 + \Delta v_y^2} = \left|\Delta v_z\right|_{x=0} \approx \left|\overline{v}_z\right|_{x=0} = v_0\frac{\overline{h}_x'}{\overline{h}_x}z = -\frac{v_0\Delta h}{lh_0}z, \tag{36}$$

$$N_s = N_{s_0} = 4\int_0^b\int_0^{h_0} k\left|\Delta v_z\right|\mathrm{d}y\mathrm{d}z \approx 4\int_0^b\int_0^{h_0} k\left|\Delta\overline{v}_z\right|\mathrm{d}y\mathrm{d}z = 4kb\int_0^{h_0}\frac{v_0\Delta h}{lh_0}z\mathrm{d}z = \frac{2\sigma_s U\Delta h}{\sqrt{3}l}, \tag{37}$$

where $\overline{v}_z$ is the average velocity in the thickness direction and $\overline{h}_x'$ is the mean value of the first derivative of the plate thickness.

3.2.5. The Minimization of the Total Power Functional. The total power functional $\dot{\Phi}$ can be expressed as

$$\dot{\Phi} = N_d + N_f + N_s. \tag{38}$$

Substituting equations (30), (35), and (37) into (38), it produces

$$\dot{\Phi} = 4.7536\sigma_s U \ln\frac{h_0}{h_1} + \frac{4m\sigma_s}{\sqrt{3}}\left[bv_R R(\theta - 2\alpha_n) + \frac{UR}{h_m}\ln\frac{\tan^2((\pi/4) + (\alpha_n/2))}{\tan((\pi/4) + (\theta/2))}\right] + \frac{2\sigma_s U\Delta h}{\sqrt{3}l}, \tag{39}$$

where v_R is the circumference velocity of the roller and α_n is the neutral angle.

The first derivative of each deformation power can be obtained from equations (30), (35), and (37).

$$\frac{\partial N_d}{\partial \alpha_n} = 4.728\sigma_s N \ln\frac{h_0}{h_1}, \tag{40}$$

$$\frac{\partial N_f}{\partial \alpha_n} = \frac{4m\sigma_s}{\sqrt{3}}\left[\frac{2UR}{h_m\cos\alpha_n} - 2v_R bR + \frac{NR}{h_m}\ln\frac{\tan^2((\pi/4) + (\alpha_n/2))}{\tan((\pi/4) + (\theta/2))}\right], \tag{41}$$

$$\frac{\partial N_s}{\partial \alpha_n} = \frac{\partial N_{s_0}}{\partial \alpha_n} = \frac{2\sigma_s N\Delta h}{\sqrt{3}l}, \tag{42}$$

where $N = (\mathrm{d}U/\mathrm{d}\alpha_n) = v_R bR\sin 2\alpha_n - v_R b(R + h_1)\sin\alpha_n$.

The derivative of equation (38) with respect to the neutral angel can be obtained as

$$\frac{\partial \dot{\Phi}}{\partial \alpha_n} = \frac{\partial N_d}{\partial \alpha_n} + \frac{\partial N_f}{\partial \alpha_n} + \frac{\partial N_s}{\partial \alpha_n} = 0. \tag{43}$$

Substituting equations (40), (41), and (42) into (43), then it leads to

$$m = \frac{N\left(2.364\sqrt{3}\,l\ln\left(h_0/h_1\right) + \Delta h\right)}{4l\left[v_R bR - \left(UR/h_m\cos\alpha_n\right) - \left(NR/2h_m\right)\ln\tan^2\left((\pi/4) + \left(\alpha_n/2\right)\right)/\tan\left((\pi/4) + (\theta/2)\right)\right]}. \tag{44}$$

By substituting equations (44) into (39), the minimum analytical solution of the total power $\dot{\Phi}$ can be obtained by using the search method. Then, rolling torque M, rolling force F, and the stress state coefficient n_σ can be obtained through

$$\begin{aligned} M &= \frac{R}{2v_R}\dot{\Phi}_{\min}, \\ F &= \frac{M}{\chi\sqrt{2R\Delta h}}, \\ n_\sigma &= \frac{\overline{p}}{2k} = \frac{F}{4blk}, \end{aligned} \tag{45}$$

where χ is the force arm coefficient, which can be determined by the literature [46]. For hot rolling, the value is about 0.5.

3.2.6. Calculation of Temperature Rise. During the rolling process of an extra-thick plate, some energy will be consumed in the form of heat, causing the plate central temperature to rise. Therefore, the influence of temperature rise should be considered in the rolling model. Taking the deformation zone as the object, the temperature rise ΔT_d caused by the rolling deformation work can be calculated by [47]

$$\Delta T_d = \frac{\dot{W}t_c}{V\rho c} = \frac{W}{m'c}, \tag{46}$$

where $\dot{W}$ and W are the total power and the total work, respectively; V is the volume of the deformation zone; $m' = V\rho$ is the weight of the workpiece in the deformation zone; c is the specific heat capacity of the material; ρ is the density of the workpiece; and t_c is the contact time that from the deformation entrance to its exit.

As some of the plastic power consumption will be stored in the workpiece in the form of dislocation and vacancy (about 2%~5%), then equation (46) should be modified as

$$\Delta T_d = \frac{\eta\dot{W}t_c}{V\rho S} = \frac{\eta W}{m'c}, \tag{47}$$

where η is the power-heat conversion coefficient, and its value range is about 0.95.

If the surface temperature of the workpiece is given, then its central temperature can be obtained as

$$T_c = T_s + \Delta T_d, \tag{48}$$

where T_s is the surface temperature of the workpiece.

In actual production, only the surface temperature of the workpiece is known. Thus, equation (48) can be used to determine the central temperature after calculating the temperature rise by equation (47).

Since the extra-thick plate is very thick, the workpiece temperature from its surface to its core is nonuniform. Thus, it is necessary to describe the temperature distribution which will affect the deformation resistance of the workpiece. The deformation resistance of the workpiece not only affected by the surface and central temperatures but also affected by the temperature distribution along the thickness direction. That is so say, the traditional method of calculating the deformation resistance is not sufficiently reasonable. The average rolling temperature should be determined by establishing a reasonable temperature field based on the surface temperature and the core temperature. Here, a simple method of establishing a temperature field is given, and the corresponding assumptions are as follows [48]:

(1) The initial temperature distribution of the workpiece is uniform. The air temperature T_f is a constant, and it is far less than the initial temperature of the workpiece.

(2) The thermal conductivity λ, density ρ, and specific heat capacity c_p of the physical parameters of the plate as well as the temperature conductivity coefficient $G = (\lambda/(\rho c_p))$ are all constant. The convective heat transfer coefficient α between the surfaces of the workpiece and the surrounding medium is the same, and it is a constant.

(3) When the cooling time τ is bigger than the critical timeτ_c (for air cooling $\tau_c = (0.2h_0^2/\alpha)$; for water cooling $\tau_c = (0.3h_0^2/\alpha)$), the temperature field enters the normal status stage.

For the extra-thick plate rolling, the temperature field can be simplified into a one-dimensional problem because the width and length of workpiece are much larger than the thickness of workpiece [48]. Under the above conditions, the upper and lower surfaces of the flat plate are cooled symmetrically, and the temperature distribution in the workpiece must be symmetrical with its central interface, as shown in Figure 7. Therefore, it is only necessary to study a half of the workpiece.

For the upper part of the workpiece, $z \geq 0$, and the one-dimensional differential equation of heat conduction and its boundary conditions can be listed as follows:

Differential equation of heat conduction:

$$\frac{\partial T_z}{\partial \tau} = G\frac{\partial^2 T_z}{\partial z^2}, \quad (0 \leq z \leq h_0, \tau \geq 0). \tag{49}$$

Initial temperature condition:

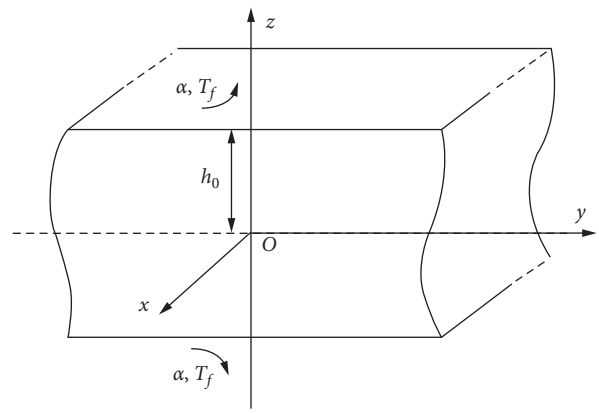

Figure 7: Temperature field analysis of an ultra-thick plate.

$$\begin{aligned} \tau &= 0, \\ T_z &= T_s. \end{aligned} \tag{50}$$

Boundary conditions:

$$\begin{aligned} &\frac{\partial T_z}{\partial z}|_{z=0} = 0, \\ &-\lambda\frac{\partial T_z}{\partial z}|_{z=0} = \alpha\left[T_z(h_0, \tau) - T_f\right]. \end{aligned} \tag{51}$$

In the author's previous research, it is found that the distribution of the temperature field in the thickness direction of an extra-thick plate can be expressed in the parabolic form [49] expressed by

$$T_z = b_1 z^2 + b_2 z + b_3. \tag{52}$$

Substituting the initial temperature condition and the boundary conditions into equation (52), it results in

$$T_z = T_c - \frac{\Delta T_d}{h_0^2} z^2. \tag{53}$$

In order to improve the accuracy of the prediction of rolling force and rolling torque, the average temperature of the workpiece $\overline{T}_z$ can be calculated in terms of the integral mean value theorem:

$$\overline{T}_z = \frac{\int_0^{h_0} T_z dz}{h_0} = T_c - \frac{\Delta T_d}{3}. \tag{54}$$

3.2.7. Mean Deformation Resistance Model. For the present study, the experimental material is one low-carbon steel, called the Q345 steel, whose yield strength is about 345 MPa after rolling. The deformation resistance model of the Q345 steel during hot deformation is [50]

$$\begin{aligned} \sigma_s &= 6310.7\overline{\varepsilon}^{0.407}\dot{\overline{\varepsilon}}^{0.115}\exp\left(-2.62 \times 10^{-3}T - 0.669\overline{\varepsilon}\right), \\ T &= T_s + 273, \end{aligned} \tag{55}$$

where $\overline{\varepsilon}$ is the equivalent strain; $\dot{\overline{\varepsilon}}$ is the equivalent strain rate; and T is the kelvin temperature.

Table 1: Calculation parameters for each rolling pass.

Pass no.	Roller velocity (v/m · s^{-1})	Entrance surface temperature (T_s/°C)	Rolling entrance thickness ($2h_0$/m)	Rolling exit thickness ($2h_1$/m)	Rolling entrance width ($2b_0$/m)	Rolling exit width ($2b_1$/m)
2	1.64	963.74	0.299	0.272	3.472	3.474
3	1.66	969.02	0.272	0.245	3.474	3.477
4	1.68	968.23	0.245	0.218	3.477	3.479
5	1.82	973.82	0.219	0.194	3.479	3.481
6	1.97	968.39	0.194	0.173	3.481	3.482

Table 2: Comparison between the calculated rolling torque with the measured ones.

Pass no.	(v_R/m · s^{-1})	(T_s/°C)	(ΔT_d/°C)	($\overline{T}_z$/°C)	Measured torque (M/kN · m)	Calculated torque (M_w/kN · m)/	Error (ΔM_w/%)	Calculated torque (M_T/kN · m)	Error (ΔM_T/%)
2	1.64	963	34.2	986.6	2640	2889	9.43	2721	3.07
3	1.66	969	38.7	994.8	2694	2826	4.89	2642	−1.93
4	1.68	968	42.4	996.5	2665	2899	8.78	2692	1.01
5	1.82	973	48.2	1006	2430	2739	12.72	2516	3.54
6	1.97	968	54.9	1005	2101	2282	8.61	2073	−1.33

Table 3: Comparison between the calculated rolling force and the measured ones.

Pass no.	(v_R/m · s^{-1})	(T_s/°C)	(ΔT_d/°C)	($\overline{T}_z$/°C)	Measured force F/kN	Calculated force (F_w/kN)	Error (ΔF_w/%)	Calculated force (F_T/kN)	Error (ΔF_T/%)
2	1.64	963	34.2	986.6	43607	48744	11.78	45914	5.23
3	1.66	969	38.7	994.8	44006	46412	5.47	43380	−1.42
4	1.68	968	42.4	996.5	43172	45871	6.25	42596	−1.33
5	1.82	973	48.2	1006	42269	43915	3.89	40367	−4.5
6	1.97	968	54.9	1005	39061	40914	4.74	37172	−4.84

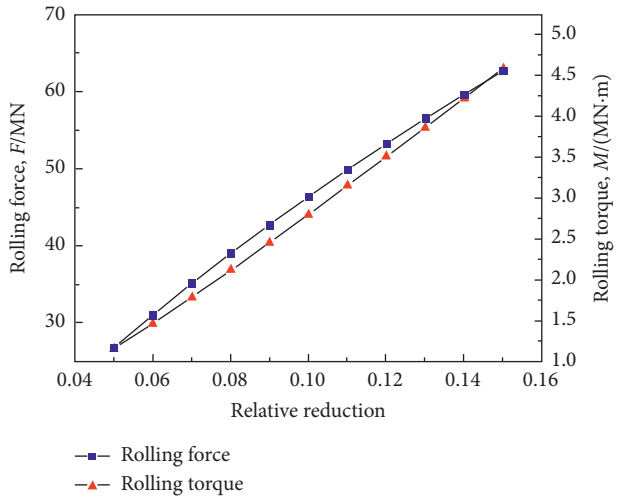

Figure 8: Influence of relative reduction on rolling torque and rolling force.

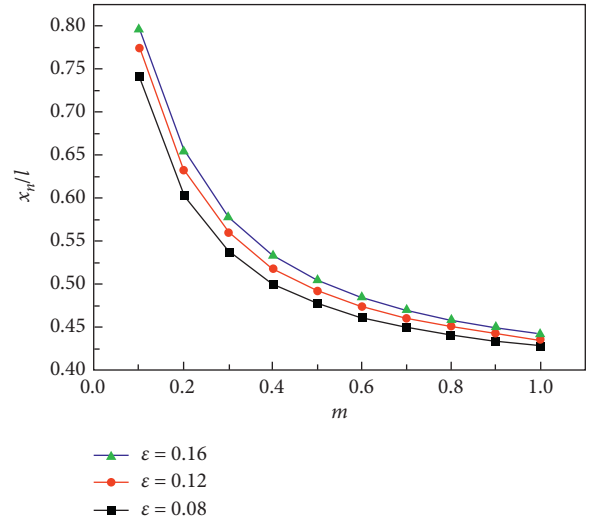

Figure 9: The relationship among the friction factor, the relative reduction, and the position of the neutral point.

By introducing the effect of the temperature rise, the mean deformation resistance model can be modified as

$$\sigma_s' = 6310.7\overline{\varepsilon}^{0.407}\dot{\overline{\varepsilon}}^{0.115}\exp\left(-2.62\times10^{-3}T' - 0.669\overline{\varepsilon}\right),$$
$$T' = \overline{T}_z + 273. \tag{56}$$

By introducing this mean deformation resistance model into equation (43), the rolling torque and rolling force accounting for the temperature rise can be obtained.

3.2.8. Experimental Verification and Parameter Analysis. The following verification is based on the rolling test data collected in a domestic factory. The diameter of the working roller of the mill is 1070 mm. The thickness, width, and length of continuous casting billet is 320 × 2050 × 3250 mm. After the first pass of shaping rolling, the steel is rolled to a thickness of 299.36 mm, and then the steel is transferred to

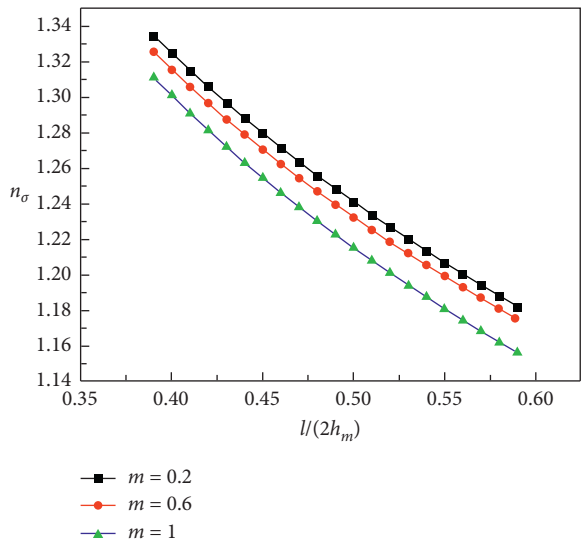

Figure 10: Relationship among the geometric factor, the friction factor, and the stress state coefficient.

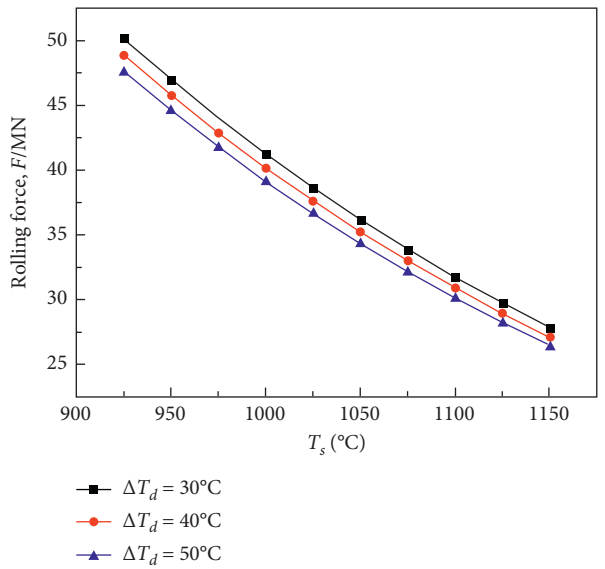

Figure 11: Comparison of the calculated rolling force with different measured workpiece surface temperature and temperature rise.

the broadside rolling stage. From the second pass to the sixth pass, the rolling passes meet the plane deformation condition because the width-to-thickness ratio of the rolling plate is greater than 10. In the present paper, the force arm coefficient χ of each pass is 0.49, 0.51, 0.53, 0.54, and 0.53, respectively. The specific parameters are listed in Table 1.

In Tables 2 and 3, the symbols M_w and F_w denote the calculated rolling torque and the rolling force when neglecting the temperature rise. The symbols M_T and F_T denote the calculated rolling torque and the rolling force when considering the temperature rise. As can be seen, both the calculated rolling torque and force coincide well with the measured ones. When neglecting the influence of temperature distribution, the maximum error of M_w and F_w is less than 12.72% and 11.78%, respectively. When the rolling model considers the influence of the temperature rise, the calculated values declined, and the maximum errors are less than 3.54% and 5.23%, respectively, which are much closer to the measure ones. Due to its high precise, the present model accounting for the temperature rise is better to be used in the rolling process optimization.

Figure 8 shows the relationship between calculated rolling torque, rolling force, and the relative reduction. As can be seen from the figure, both the rolling torque and rolling force have a positive linear correlation with the relative reduction.

Figure 9 is the change curve among the friction factor, the relative reduction, and the neutral point position. With the decrease in friction factor or the increase in reduction, the neutral points move to the exit section. When $(x_n/l) \leq 0.6$, a small change in the friction factor will lead to a large change in the neutral point position, which indicates that the position of the rolling equilibrium point changes greatly, which is not conducive to stable rolling. Therefore, rolling in this range should be avoided in actual production.

Figure 10 shows the influence of the geometric factor $(l/(2h_m))$ and the friction factor on the stress state coefficient n_σ. As can be seen, the n_σ decreases with the increase in $(l/(2h_m))$. Even if the friction factor is the largest $m = 1$, the effect on the stress state coefficient is very small, almost negligible.

Figure 11 shows that the calculated rolling force decreases with the increase in surface temperature or temperature rise. Because of the temperature rise embedded in the deformation resistance model, the change of temperature rise has a certain influence on the rolling force. Therefore, it can be concluded that when establishing a prediction model of rolling force with high prediction accuracy, the influence of temperature rise should be considered carefully.

4. Conclusions

(1) In this paper, the Mises yield criterion is linearized in geometry, and a linear CA yield criterion is proposed. Also, the formula of its specific plastic power is derived, which is a function of σ_s, $\dot{\varepsilon}_{\max}$, and $\dot{\varepsilon}_{\min}$. Using the proposed linear criterion formula to replace the nonlinear formula of Mises, the integral difficulty in the power calculating is solved.

(2) Verification results show that the locus of the CA yield criterion is between the Tresca yield criterion locus and TSS yield criterion locus, which not only realizes the linear approximation of Mises but also the locus is similar to the change trend of each test data.

(3) Using the CA yield criterion, a rolling force model is established. The maximum rolling torque error and maximum rolling force error without considering temperature rise are, respectively, 12.72% and 11.78%, while those considering the temperature rise are 3.54% and 5.23%.

(4) The rolling force model derived by the CA yield criterion and accounting for the temperature rise can provide reasonable results, which can be used in the design and optimization of rolling process.

Data Availability

All data generated or analyzed during this study are included within this article.

Conflicts of Interest

The authors declare that they have no conflicts of interest.

Acknowledgments

This research was supported by the National Natural Science Foundation of China (grant nos. 52074187, U1960105, and 51504156), the Outstanding Youth Foundation of Jiangsu Province (grant no. BK20180095), and the Prospective Applied Research from the Technological Innovation Project of Key Industry of Suzhou (grant no. SYG201806).

References

[1] C. A. Coulomb, "Essai sur une application des règles de maximis & minimis à quelques problèmes de statique, relatifs à l'architecture," *Mémoires, Divers Savants*, vol. 7, pp. 343–382, 1776.

[2] H. Tresca, "On the flow of solid bodies subjected to high pressures," *Comptes Rendus De l'Académie Des Sciences*, vol. 59, p. 754, 1864.

[3] R. Von Mises, "Mechanik der festen korper im plastisch deformablen Zustand," *Nachrichten Von Der Gesellschaft Der Wissenschaften Zu Göttingen, Mathematisch-Physikalische Klasse*, vol. 1, pp. 582–592, 1913.

[4] R. V. Mises, "Mechanik der plastischen formänderung von kristallen," *ZAMM-Zeitschrift Für Angewandte Mathematik Und Mechanik*, vol. 8, no. 3, pp. 161–185, 1928.

[5] R. Hill, *The Mathematical Theory of Plasticity*, Clarendon Press, Oxford, UK, 1950.

[6] M.-H. Yu, "Advances in strength theories for materials under complex stress state in the 20th century," *Applied Mechanics Reviews*, vol. 55, no. 3, pp. 169–218, 2002.

[7] M.-H. Yu, "Twin shear stress yield criterion," *International Journal of Mechanical Sciences*, vol. 25, no. 1, pp. 71–74, 1983.

[8] D. W. Zhao and G. F. Li, "The surface integral to axisymmetric drawing through elliptic-die profile," *Engineering Mechanics*, vol. 11, no. 4, pp. 131–136, 1994, in Chinese.

[9] D. W. Zhao, J. Z. Xu, and H. Yang, "Application of twin shear stress yield criterion in axisymmetrical indentation of a semi-infinite medium," in *Proceedings of International Symposium on Strength Theory*, pp. 1079–1084, New York, NY, USA, January 1998.

[10] M. H. Yu, *A New System of Strength Theory*, Xian Jiaotong University Print, Xi'an, China, 1992, in Chinese.

[11] M. H. Yu, *Unified Strength Theory and its Application*, Xi'an Jiaotong University Press, Xi'an, China, 1995, in Chinese.

[12] S. Q. Li, H. L. Li, L. B. Zhang et al., "The generalized double $\tau 2$ yield criterion," *Journal of Hebei University (Natural Science Edition)*, vol. 22, no. 3, pp. 229–233, 2002, in Chinese.

[13] D. W. Zhao, X. H. Liu, and G. D. Wang, "Yield criteria that rely on Tresca and the mean of the double shear yield function," *Journal of Northeastern University (Natural Science Edition)*, vol. 23, no. 10, pp. 43–52, 2002, in Chinese.

[14] O. Cazacu and F. Barlat, "A criterion for description of anisotropy and yield differential effects in pressure-insensitive metals," *International Journal of Plasticity*, vol. 20, no. 11, pp. 2027–2045, 2004.

[15] X.-K. Zhu and B. N. Leis, "Average shear stress yield criterion and its application to plastic collapse analysis of pipelines," *International Journal of Pressure Vessels and Piping*, vol. 83, no. 9, pp. 663–671, 2006.

[16] M. Song and Y.-H. He, "A unified criterion for yielding behavior of metallic glasses," *Journal of Central South University of Technology*, vol. 18, no. 1, pp. 1–5, 2011.

[17] X. R. Hu and X. M. Fan, "The triple-shear unified yield criterion and its applications," *Applied Mechanics and Materials*, vol. 94–96, pp. 1129–1140, 2011.

[18] A. S. Khan, S. Yu, H. Liu et al., "Deformation induced anisotropic responses of Ti-6Al-4V alloy part II: a strain rate and temperature dependent anisotropic yield criterion," *International Journal of Plasticity*, vol. 38, no. 4, pp. 14–26, 2012.

[19] D. Banabic, L. Lazarescu, and D. S. Comsa, "Predictive performances of FLC using marciniak-kuczynski model and modified maximum force criterion," *Key Engineering Materials*, vol. 651–653, pp. 96–101, 2015.

[20] Y. Lou and J. W. Yoon, "A shear ductile fracture criterion for metal forming"" *Journal of Physics: Conference Series*, vol. 734, no. 3, pp. 132–137, 2016.

[21] A. Werber, M. Liewald, W. Nester et al., "Development of a new failure prediction criterion in sheet metal forming," *International Journal of Material Forming*, vol. 7, no. 4, pp. 395–403, 2014.

[22] S. I. Oh and S. Kobayashi, "An approximate method for a three-dimensional analysis of rolling," *International Journal of Mechanical Sciences*, vol. 17, no. 4, pp. 293–305, 1975.

[23] K. Kato, T. Murota, and T. Kumagai, "Flat-rolling fo rigid-perfectly plastic solid bar by the energy method," *Journal of the Japan Society for Technology of Plasticity*, vol. 21, pp. 359–369, 1980.

[24] A. Parghazeh and H. Haghighat, "Prediction of central bursting defects in rod extrusion process with upper bound analysis method," *Transactions of Nonferrous Metals Society of China*, vol. 26, no. 11, pp. 2892–2899, 2016.

[25] J. Cao, Y. Liu, F. Luan et al., "The calculation of vertical rolling force by using angular bisector yield criterion and Pavlov principle," *The International Journal of Advanced Manufacturing Technology*, vol. 86, no. 9–12, pp. 2701–2710, 2016.

[26] D. H. Zhang, Y. M. Liu, J. Sun et al., "A novel analytical approach to predict rolling force in hot strip finish rolling based on cosine velocity field and equal area criterion," *The International Journal of Advanced Manufacturing Technology*, vol. 84, no. 5–8, pp. 843–850, 2016.

[27] Y.-M. Liu, G.-S. Ma, D.-W. Zhao, and D.-H. Zhang, "Analysis of hot strip rolling using exponent velocity field and MY criterion," *International Journal of Mechanical Sciences*, vol. 98, pp. 126–131, 2015.

[28] W. Peng, D. Zhang, and D. Zhao, "Application of parabolic velocity field for the deformation analysis in hot tandem rolling," *The International Journal of Advanced Manufacturing Technology*, vol. 91, no. 5–8, pp. 2233–2243, 2016.

[29] H. Y. Wang, D. W. Zhao, and D. H. Zhang, "Analysis of vertical rolling force with GM yield criterion and anti-

symmetric parabola dog-bone shapes," *Applied Mechanics and Materials*, vol. 775, no. 1, pp. 34–38, 2015.

[30] S. Zhang, B. Song, X. Wang, D. Zhao, and X. Chen, "Deduction of geometrical approximation yield criterion and its application," *Journal of Mechanical Science and Technology*, vol. 28, no. 6, pp. 2263–2271, 2014.

[31] S. H. Zhang, L. Deng, Q. Y. Zhang, Q. H. Li, and J. X. Hou, "Modeling of rolling force of ultra-heavy plate considering the influence of deformation penetration coefficient," *International Journal of Mechanical Sciences*, vol. 159, pp. 373–381, 2019.

[32] B. Akgöz and Ö. Civalek, "Buckling analysis of functionally graded microbeams based on the strain gradient theory," *Acta Mechanica*, vol. 224, no. 9, pp. 2185–2201, 2013.

[33] B. Akgöz and Ö. Civalek, "A microstructure-dependent sinusoidal plate model based on the strain gradient elasticity theory," *Acta Mechanica*, vol. 226, no. 7, pp. 2277–2294, 2015.

[34] F. Ebrahimi, M. R. Barati, and Ö. Civalek, "Application of Chebyshev-Ritz method for static stability and vibration analysis of nonlocal microstructure-dependent nanostructures," *Engineering with Computers*, vol. 36, no. 3, pp. 953–964, 2020.

[35] I. Le May, *Principles of Mechanical Metallurgy*, Elsevier, North-Holland, New York, NY, USA, 1981.

[36] W. Lode, "Versuche über den einfluß der mittleren hauptspannung auf das fließen der metalle eisen, Kupfer und Nickel," *Zeitschrift Für Physik*, vol. 36, no. 11-12, pp. 913–939, 1926.

[37] J. M. Lessells and C. W. MacGregor, "Combined stress experiments on a nickel-chrome-molybdenum steel," *Journal of the Franklin Institute*, vol. 230, no. 2, pp. 163–181, 1940.

[38] P. M. Naghdi, F. Essenburg, and W. Koff, "An experimental study of initial and subsequent yield surfaces in plasticity," *Journal of Applied Mechanics*, vol. 25, pp. 201–209, 1957.

[39] W. A. Maxey, "Measurement of yield strength in the mill expander," in *Proceedings of the Fifth Symposium on Line Pipe Research*, Houston, TX, USA, November 1974.

[40] E. A. Davis, "Yielding and fracture of medium-carbon steel under combined stress," *Journal of Applied Mechanics*, vol. 67, pp. 13–24, 1945.

[41] J. Marin and L. W. Hu, "Biaxial plastic stress-strain relations of a mild steel for variable stress ratios," *Journal of Applied Mechanics*, vol. 78, pp. 499–509, 1956.

[42] M. Ros and A. Eichinger, "Versuche zur klaerung der frageder bruchefahr III, mettalle, eidgenoss," *Material Pruf. Und Versuchsantalt Industriell Bauwerk Und Geerbe, Diskussionsbericht*, vol. 34, pp. 3–59, 1929.

[43] S. H. Zhang, X. N. Wang, D. W. Zhao et al., "Analysis of broadside rolling force for hot heavy plate using angle bisector yield criterion," *Journal of University of Science and Technology Liaoning*, vol. 39, no. 6, pp. 417–423, 2016, in Chinese.

[44] Y. H. Pang and Z. Z. Du, *Material Science Textbook for Higher Education*, Northwestern Polytechnical University, Xi'an, China, 2011.

[45] D.-W. Zhao, Y.-J. Xie, X.-H. Liu, and G.-D. Wang, "Three-dimensional analysis of rolling by twin shear stress yield criterion," *Journal of Iron and Steel Research International*, vol. 13, no. 6, pp. 21–26, 2006.

[46] J. N. Harri, *Mechanical Working of Metals, Theory and Practice*, A. Wheaton &Co., Ltd, Exeter, England, 1st edition, 1983.

[47] D. W. Zhao, *Principle and Application of Integral Linearization of Forming Energy Rate*, Metallurgical Industry Press, Beijing, China, 2012, in Chinese.

[48] M. Yu, *Research and Application of Analytical Solution for Temperature Field in Accelerated Cooling Process of Plate*, Northeastern University, Shenyang, China, 2008.

[49] S. H. Zhang, D. W. Zhao, N. J. Liu et al., "The temperature field is decomposed in the normal cooling stage after rolling," *Engineering Mechanics*, vol. 30, no. B06, pp. 363–366, 2013.

[50] Q. J. Chen, Y. L. Kang, H. P. Hong et al., "Finite element simulation of rolling process of low alloy wide sheet," *Journal of Plastic Engineering*, vol. 12, pp. 163–167, 2015, in Chinese.